Title

A combined hiPSC-derived endothelial cell and in vitro microfluidic platform for assessing biomaterial-based angiogenesis

Authors

Natividad-Diaz, Sylvia L
Browne, Shane
Jha, Amit K
et al.

Publication Date

2019-02-01

DOI

10.1016/j.biomaterials.2018.11.032

Peer reviewed

HHS Public Access

Author manuscript

Biomaterials. Author manuscript; available in PMC 2020 February 01.

Published in final edited form as:

Biomaterials. 2019 February ; 194: 73–83. doi:10.1016/j.biomaterials.2018.11.032.

A combined hiPSC-derived endothelial cell and *in vitro* microfluidic platform for assessing biomaterial-based angiogenesis

Sylvia L. Natividad-Diaz[1], **Shane A. Browne**[1], **Amit K. Jha**[1,2], **Zhen Ma**[1,†], **Samir Hossainy**[1,2], **Yosuke K. Kurokawa**[3], **Steven C. George**[4], and **Kevin E. Healy**[1,2,*]

[1]Department of Bioengineering, University of California-Berkeley, Berkeley, California, United States

[2]Department of Materials Science and Engineering, University of California-Berkeley, Berkeley, California, United States

[3]Department of Biomedical Engineering, Washington University in St Louis, MO, USA

[4]Department of Biomedical Engineering, University of California-Davis, Davis, California, United States

Abstract

Human induced pluripotent stem cell (hiPSC) derived angiogenesis models present a unique opportunity for patient-specific platforms to study the complex process of angiogenesis and the endothelial cell response to biomaterial and biophysical changes in a defined microenvironment. We present a refined method for differentiating hiPSCs into a CD31+ endothelial cell population (hiPSC-ECs) using a single basal medium from pluripotency to the final stage of differentiation. This protocol produces endothelial cells that are functionally competent in assays following purification. Subsequently, an *in vitro* angiogenesis model was developed by encapsulating the hiPSC-ECs into a tunable, growth factor sequestering hyaluronic acid (HyA) matrix where they formed stable, capillary-like networks that responded to environmental stimuli. Perfusion of the networks was demonstrated using fluorescent beads in a microfluidic device designed to study angiogenesis. The combination of hiPSC-ECs, bioinspired hydrogel, and the microfluidic platform creates a unique testbed for rapidly assessing the performance of angiogenic biomaterials.

[*]**Corresponding author:** Kevin E. Healy, kehealy@berkeley.edu.

[†]Current affiliation: Department of Biomedical & Chemical Engineering, Syracuse Biomaterials Institute, Syracuse University, Syracuse, NY

7. Declarations of interest

KEH has a financial relationship with Organos Inc. and both he and the company may benefit from commercialization of the results of this research.

8. Data Availability Statement

The raw and processed data required to reproduce these findings will be made available via contact with corresponding author.

Keywords

human induced pluripotent stem cells (hiPSCs); hiPSC-derived endothelial cells (hiPSC-ECs); differentiation; hyaluronic acid; hydrogel; *in vitro* angiogenesis model

1. Introduction

Angiogenesis is a complex process that is involved in disease progression and tissue repair. The multifaceted, spatiotemporal mechanisms of angiogenesis along with the relatively high cost and technical skill level associated with *in vivo* studies make it difficult to rapidly and efficiently evaluate the efficacy of both biomaterials and molecular therapies targeting vascular network formation [1–11]. *In vitro* models provide a less expensive, more controlled, and reproducible platform for better quantification of isolated angiogenic processes in response to biomaterial, biochemical, or biophysical stimuli [3, 11–15].

Biomaterials designed for angiogenesis have typically exploited key extracellular matrix (ECM) parameters such as mechanical properties, ligand density of integrin-engaging peptides, growth factor presentation, and cell-mediated matrix metalloproteinase (MMP) degradation. While ECM-derived materials such as collagen and gelatin offer intrinsic support for encapsulated cells, control over matrix parameters is somewhat limited [16–19]. Decellularized ECM (dECM) are often used for tissue-specific applications, and provide an ideal structure of ECM proteins and glycosaminoglycans (GAGs) to stimulate cell proliferation and migration [20, 21]. However, given that dECM are derived from natural sources, engineering control over key parameters remains a challenge. In contrast, synthetic materials provide a wide design space for control over the aforementioned key parameters, but lack the intrinsic bioactivity vascular cells require to self-assemble into networks. Thus, semisynthetic matrices (sECM), where biopolymers are modified to impart controlled and defined bioactivity, provide an ideal platform to control the formation of vascular networks [15]. In this regard, hyaluronic acid (HyA) stands out as a readily modifiable biopolymer to construct defined sECM [5, 22–24].

Although current *in vitro* angiogenesis models employing biomaterials have provided great advances and insight into this process, many models continue to rely on primary endothelial cells (ECs) (human umbilical vein endothelial cells [HUVEC], human microvascular endothelial cells [HMVEC], human aortic endothelial cells [HAEC], etc) or immortalized cell lines [3, 4, 9, 11, 25–29]. Primary ECs are plagued by patient source variation, and in some cases genetic diversity, so that patients from different backgrounds (gender, age, race/ethnicity, etc) are not well represented in the models. Furthermore, primary cell lines are limited in supply and are notoriously difficult to culture and expand, thus failing to provide a sustainable source for *in vitro* studies [3, 11, 28, 30]. Additionally, HUVECs have a tendency to form unstable capillary structures *in vitro* that quickly and spontaneously regress making it difficult to assess the impact of biomaterial design on study outcomes. Many studies include secondary stromal cells, often from a different patient (e.g. allogenic model), to stabilize these capillary-like networks [25, 26, 31–33], which adds confounding factors associated with the different genetic backgrounds.

In contrast to primary endothelial cells, human induced pluripotent stem cell (**hiPSC**) derived endothelial cells (**hiPSC-ECs**) have the potential to provide a limitless supply of patient-specific vascular cells to research pathological angiogenesis, vascular diseases, and matrix-assisted cell transplantation for regeneration of ischemic tissues [1, 3, 11, 13, 30]. More recently refined endothelial cell differentiation protocols include both CD31+ and CD34+ populations, which negates the need for additional co-cultured stromal cells to support the hiPSC-EC's function and formed vessel structure [34]. Incorporating hiPSC-ECs into angiogenesis models provides a patient-specific platform to study *in vitro* the complex process of biomaterial-based angiogenesis.[3, 11, 14, 35].

In this work we present a method for differentiating a CD31+ endothelial cell population from hiPSCs, a 3D angiogenesis model employing these cells, and a combined microfluidic testbed for studying angiogenesis *in vitro*. A schematic diagram of our workflow is shown in Figure 1(a). To develop this model and assess the behavior of these hiPSC-ECs, we used a growth factor sequestering hyaluronic acid (HyA) matrix to promote cell survival and maintenance of lineage-specific function [36–38]. The HyA hydrogel synthesis for hiPSC-EC encapsulation included an integrin binding peptide (bsp-RGD(15)) [39], high molecular weight heparin as a growth-factor presenting agent [36], and a MMP-degradable peptide crosslinker. HyA offers many benefits as a matrix to support hiPSC-ECs, since it is a naturally occurring biopolymer that is biocompatible, biodegradable, non-immunogenic, and has been shown to promote cell migration, proliferation, and angiogenesis in wound healing processes [5, 6, 10, 24, 36–38, 40, 41]. The hiPSC-ECs were encapsulated within the HyA matrix, using different media and growth factor combinations, and their ability to respond to changes in their microenvironment was demonstrated with dynamic changes in capillary-like network formation and nitric oxide production similar to physiological angiogenesis. The dependence of network formation on proangiogenic signaling was further demonstrated by treatment with a small-molecule VEGFR2/FGFR inhibitor which eliminated network formation and permitted assessment of the toxicity of the compound. We then incorporated the *in vitro* angiogenesis model containing the HyA matrix and hiPSC-ECs within a tri-chamber microfluidic device that mimicked vascular flow and demonstrated perfusion of hollow capillary tube networks.

2. Materials and Methods

2.1 Human Pluripotent Stem Cell Culture and Maintenance

Human induced pluripotent stem cell (hiPSC) line WTC and human embryonic stem cell (hESC) line H9 were grown on plates coated with growth factor-reduced Matrigel (Corning) at 15,000-20,000 cells/cm^2 and were fed Essential 8 Medium (ThermoFisher). The cells were passaged every 3 days and 10 uM rho-associated protein kinase (ROCK) inhibitor (Y-27632, STEMCELL Technologies) was added to the culture medium for the first 24 hours after passaging.

2.2 Modified Protocol for hPSC-Endothelial Cell Differentiation

The modified protocol for endothelial cell differentiation in 2D culture developed in this study is summarized in Figure 1(a). First, the human pluripotent stem cells were passaged

onto plates coated with growth factor-reduced Matrigel (Corning) at 25,000-30,000 cells/cm^2 and fed Essential 8 Medium supplemented with 10 uM ROCK inhibitor (day -2). The medium was replaced the next day (day -1) with Essential 8 without ROCK inhibitor. The cells were grown to approximately 80% confluency which occurs on day 0 with this initial seeding density. Differentiation was initiated on day 0, by feeding the cells Essential 8 Medium supplemented with 6 uM CHIR 99021 (STEMCELL Technologies). Endothelial lineage specification was started on day 2 by the addition of Essential 8 Medium supplemented with 10 ng/ml BMP4 (R&D systems), 50 ng/ml VEGF-A_{165} (R&D Systems), and 10 uM SB431542 (TOCRIS). The cells were fed this medium (E8BVi) everyday for 3 more days up to the final stage of differentiation on day 5. After day 5, the cells were magnetically sorted for CD31+ expression and expanded in EGM2. (Commercially available media compositions are summarized in Supplementary Table 1)

2.3 Flow Cytometry Analysis

Cells were dissociated using TrypLE (ThermoFisher) with a 7-minute incubation in 37°C (5% CO_2) and quenched with EGM2 (1:5 enzyme to EGM2). The cells were then centrifuged at 1200 rpm for 5 minutes and the supernatant was removed. The cells were then washed with PBS and fixed with 4% paraformaldehyde for 10 minutes. The sample was centrifuged to remove PFA and then washed twice with PBS. The sample was resuspended in FACSB10 buffer [42] and stained with the fluorescently labeled antibodies listed in Table 2. The sample and antibodies were incubated overnight at 4°C. Samples were analyzed with a Beckman Coulter FC500 flow cytometer. The data was analyzed with Kaluza software (Beckman Coulter) and gating was based on corresponding isotype controls.

2.4 CD31+ Endothelial Cell Magnetic-Activated Cell Sorting (MACS)

Magnetic-activated cell sorting (MACS) was done on day 5 of differentiation or the following day to avoid over-confluence of cultures, which would decrease purity of the positively isolated population. Endothelial cells were magnetically sorted with Dynabeads M-280 Sheep Anti-Mouse (Invitrogen, Carlsbad, CA) coated with primary mouse anti-human CD31 antibody (Invitrogen) at a ratio of 5:1 beads to cells. Prior to sorting, the dynabeads were washed twice with sterile FACSB10 buffer [42] with a DynaMag-15 magnet (Invitrogen). The beads were resuspended in 200 uL FACSB10 and incubated with mouse anti-human CD31 antibody (1:50) for 30 minutes at room temperature with gentle rocking. Antibody conjugated beads were then washed twice with FACSB10 and resuspended in 500 uL FACSB10. Cells were singularized using TrypLE with a 7-minute incubation period (37°C, 5% CO_2) and quenched with EGM2 (1:5 enzyme to EGM2). The cells were then centrifuged at 1200 rpm for 5 minutes and the supernatant was removed. The antibody-conjugated beads were then mixed with the cells and incubated at room temperature with gentle rocking for 30 minutes. The CD31+ cells were then isolated from the rest of the population with the DynaMag-15 magnet with two washes consisting of FACSB10 and one wash with EGM2. The isolated, bead-bound endothelial cells were then resuspended in EGM2 with 10uM Rock Inhibitor. The cells were seeded at 150,000 cells/cm^2 on 0.2% Gelatin coated TCPS plates. The cells were fed EGM2 the following day and every two days thereafter.

2.5 Fluorescence Microscopy

Cells were rinsed with PBS and fixed with 4% PFA for 10 minutes. They were then washed with PBS and stained sequentially with primary and secondary antibodies in 1% BSA buffer for either 2 hours at room temperature or overnight at 4°C (antibodies are listed in Supplemental Table 2). The samples were then washed twice with PBS. Fluorescent and phase contrast images were taken on a Nikon Eclipse TE300 microscope with a Hamamatsu C11440 digital camera and Zen lite software (Carl Zeiss, Thornwood, NY).

2.6 Reverse Transcription Quantitative Polymerase Chain Reaction (RT-qPCR)

Total RNA was isolated and purified using the RNeasy Mini Kit (Qiagen, Germantown, MD) according to manufacturer specifications, including the DNase I treatment (RNase-Free DNase Set, Qiagen). A NanoDrop™ 2000/2000c spectrophotometer (ThermoFisher) was used to measure RNA concentration. RNA (1-2 ug) was reverse transcribed to cDNA using the SuperScript III Reverse Transcriptase kit (Invitrogen) with Oligo(dT) primer according to manufacturer specifications. Real-time quantitative PCR was done on 10 ng of cDNA from each sample with RT2 SYBR Green Mastermix (Qiagen) on a StepOnePlus thermocycler (Applied Biosystems). The primers for the tested genes are listed in Supplemental Table 3, GAPDH and HSP90AB1 were used as endogenous housekeeping controls.

2.7 DiI Ac-LDL Uptake Assay

Live, CD31+ purified cells were incubated with DiI fluorescent dye-labeled acetylated low-density lipoprotein (DiI-ac-LDL) (ThermoFisher) at 10 ug/mL in EGM2 for 4 hours at 37°C, 5% CO_2. The cells were then rinsed with PBS and imaged on a Nikon Eclipse TE300 microscope.

2.8 Matrigel Angiogenesis Assay

CD31+ purified endothelial cells were seeded at 62,500 cells per cm^2 on 100 uL growth-factor reduced Matrigel in a 96-well plate in EGM2. Tube formation was observed with Nikon Eclipse TE300 phase contrast microscope after 24 hours, 48 hours, and 72 hours of incubation.

2.9 Hyaluronic Acid (HyA)-Based Matrix Synthesis

2.9.1 Acrylated HyA Synthesis—HyA was purchased from LifeCore Biomedical with a reported molecular weight of 500kDa, which was determined through viscosity measurements by the manufacturer. The HyA was modified to carry acrylate groups using a previously reported method [38]. Briefly, the hyaluronic acid was dissolved in deionized water overnight to form a 3 mg/mL solution. A 30 molar excess of adipic acid dihydrazide (ADH) was added to the solution and the pH was adjusted to 6.8 using 0.1 M NaOH and 0.1 M HCl. Next, 1-Ethyl-(3-dimethylaminopropyl)carbodiimide hydrochloride (EDC) (Fisher Scientific) and 1-Hydroxybenzotriazole hydrate (HOBt) (Sigma-Aldrich) were dissolved separately at 3 mmol in DMSO/DI water (1:1 volume ratio, 3 mL) and sequentially added to the reaction solution. The solution pH was then adjusted to 6.8 and maintained for 4 hours before letting the reaction proceed overnight. The solution was exhaustively dialyzed for 3

days in 10 kDa molecular weight cut-off (MWCO) dialysis tubes (Spectrum Labs) against 1 g/L NaCL in DI water for the first two days and pure DI water the third day. Following dialysis, NaCl was added to form a 5 mg/mL solution which was then precipitated in 100% ethanol. The precipitated HyA-ADH was pelleted by centrifugation and re-dissolved in DI water. The solution was again dialyzed using the same method. To generate acrylate groups on the HyA, 700 mg of N-Acryloxysuccinimide (NAS) (Acros Organics) was reacted overnight with the HyA-ADH solution (300 mg, 100 mL DI water). The solution was dialyzed following the same method and then lyophilized for at least 3 days to remove all water and stored at −20°C. Previous reports confirmed with proton (^{1}H) NMR that ~30% of the available carboxyl groups were conjugated with acrylated groups [38].

2.9.2 Synthesis of Thiolated Heparin—Thiolated Heparin was synthesized using a previously reported method [38]. Briefly, heparin (50 mg) (Sigma Aldrich) was dissolved in DI water to form a 5 mg/mL solution which was reacted with an excess amount of cysteamine (76 mg) and the solution pH was adjusted to 6.8. Next, 1-Ethyl-(3-dimethylaminopropyl) carbodiimide hydrochloride (EDC) (Fisher Scientific) and 1-Hydroxybenzotriazole hydrate (HOBt) (Sigma-Aldrich) were dissolved separately at 3 mmol in DMSO/DI water (1:1 volume ratio, 0.5 mL) and sequentially added to the reaction solution. The solution pH was then adjusted to 6.8 and maintained for 5 hours before letting the reaction proceed overnight. A 10-fold molar excess of tris (2-carboxyethyl) phosphine (TCEP) was added to reduce any disulfide bonds that may have formed between thiol groups. The solution pH was adjusted to 5.0 and then dialyzed following the same method as described for the synthesis of acrylated HyA. The thiolated heparin was lyophilized for at least 3 days and stored at −20°C.

2.9.3 Gelation of HyA for Encapsulation of hiPSC-EC—The gelation procedure for the HyA hydrogel was previously reported [36–39]. To promote cellular adhesion, HyA was conjugated with an integrin binding peptide, bsp-RGD(15) with the amino acid sequence CGGNGEPRGDTYRAY [39, 43]. HyA-RGD was synthesized by reacting 10 mg of bsp-RGD(15) to 25 mg AcHyA in 10 mL of DI water at room temperature. To make a 3 wt% hydrogel HyA (13.3 mg/mL), HyA-RGD (20 mg/mL), and heparin-SH (0.03 wt%) were dissolved in 0.3 mL of triethanolamine buffer (TEA; 0.3M, pH 8) and incubated at 37°C for 30 minutes. For gels with exogenous growth factor addition, VEGF-A_{165} (5 ug/mL) or TGF-β1 (1 ug/mL) was incubated with the solution for 30 minutes at 4°C. Sorted CD31+ WTC hiPSC-ECs were then gently mixed into the solution at a concentration of 3×10^6 cells/mL. Hydrogels were generated by in situ crosslinking with an MMP-13 cleavable peptide sequence CQPQGLAKC (3 mg, 50 μL TEA buffer). The reported shear modulus (G') of the 3 wt% HyA hydrogel was 850 Pa and a 2 wt% hydrogel was reported to have a shear modulus (G') of 170 Pa [38]. Therefore, the 3wt% HyA hydrogel was referred to as **HyA-850** and the 2 wt% hydrogel was **HyA-170**.

2.10 Hydrogel Immunofluorescence and confocal microscopy

Cells encapsulated within the hydrogel were rinsed with PBS and fixed with 4% PFA for 30 minutes and permeabilized for 5 minutes with 0.1% Triton. The samples were then rinsed three times with PBS and blocked with 3% BSA for 30 minutes. They were then stained

with 1:200 primary anti-human CD31 (Supplemental Table 2) and 1:200 Actin-stain 555 phalloidin (Cytoskeleton, Inc.) in PBS overnight at 4°C. Next, the samples were washed in triplicate with PBS and stained with Alexa Fluor 488 goat anti-mouse secondary antibody (1:200 in PBS) and incubated overnight at 4°C. The samples were then washed three times with PBS. Prior to imaging, cell nuclei were stained with DAPI (Invitrogen) for 5 minutes and washed once with PBS. Fluorescent images were taken with a Prairie Technologies Swept Field Confocal (SFC) microscope (Prairie Technologies, Middleton, WI).

2.11 Angiogenesis Analysis

Tube formation in the hiPSC-EC hydrogel samples was quantified with the ImageJ Angiogenesis Analyzer plugin [44] by measuring total branching and segment lengths (termed total network length) in confocal images. To help the software distinguish between tube structures and background, the images were converted to binary images. The Angiogenesis Analysis software was then used to convert the binary image to a "branching skeleton", or binary tree, and the total length was measured using the "Analyze Binary Tree" function.

2.12 Nitric Oxide Assay

The presence of nitric oxide released into the culture medium by the encapsulated hiPSC-ECs was detected using the Griess Reagent System (Promega) according to manufacturer specifications. This assay measures the concentration of nitrite, a stable degradation product of nitric oxide, present in the sample culture medium. Hydrogel samples were fed every other day with EGM2, which was collected and tested at days 3, 7, and 14.

2.13 Angiogenesis Inhibition Assay

The angiogenesis inhibition assay was performed with a ten-fold dilution series of the small molecule VEGFR2/FGFR inhibitor SU5402 (Sigma) in EGM2 and feeding it to hiPSC-ECs encapsulated in 3 wt% HyA hydrogel on day 1 to day 7. The samples were fixed with 4% PFA and stained for F-actin and DAPI, as described above. Fluorescent images were taken with a Prairie two photon/confocal microscope and analyzed with the ImageJ Angiogenesis Analyzer plugin. Nonlinear regression analysis of the dose-response curve to calculate IC_{50} was performed with Graphpad Prism 6 (data represents a fit to three experimental replicates).

2.14 Perfusion Analysis

The 3wt% HyA hydrogel with 3×10^6 cells/mL (WTC hiPSC-ECs) was loaded with a P200 positive pressure pipette into a 3-chamber microfluidic device shown in **Figure 7(a-1)** and described previously [25, 45]. The microfluidic platform was designed to mimic vascular flow and originally consisted of two fluidic channels separated by a central channel of 12 consecutively connected diamond tissue chambers. The central channel containing the tissue chambers had ports at each end where the cell-hydrogel solution was loaded. The fluidic channels connected on either side of the tissue chamber via a single connecting pore designed to act as a capillary burst microvalve to keep liquid from leaking out. The samples were fed EGM2 every other day through gravity-fed flow from filterless P200 pipette tips.

To test perfusion, the samples were fixed on day 14 and the device was loaded with 2 μm diameter fluorescent microbeads (Fluospheres, Invitrogen). Fluorescent images and videos were taken at a 100 fps on the Prairie Technologies Swept Field Confocal (SFC) microscope (Prairie Technologies, Middleton, WI).

2.15 Statistical Analysis

All quantitative measurements were performed at least in triplicate samples and values are expressed as mean ± standard deviation (SD). One-way ANOVA with post-hoc Tukey tests were used to compare treatment groups and $p<0.05$ was used to assess statistical significance.

3. Results

3.1 hiPSC-EC Differentiation

The protocol timeline for hiPSC-EC differentiation developed in this study is summarized in Figure 1(b). The protocol is primarily based on the SMAD and MAPK signaling pathways, which are active during embryonic vasculogenesis and angiogenesis [46–48]. Mesoderm formation was initiated on day 0 by supplementing E8 media with the small molecule, CHIR99021, which inhibited the serine/threonine protein kinase, GSK3 [49]. On day 2, E8 was supplemented with BMP4, VEGF-A, and the small molecule SB431542. The inherent TGF-β1 and supplemented BMP4 bind the ALK1/5 and ALK3/6 transmembrane receptors respectively, and activate the SMAD1/5 signaling pathway, which promotes endothelial cell lineage specification and proliferation [50–52]. However, TGF-β1 also activates the SMAD 2/3 pathway via ALK5 activation, which inhibits endothelial cell proliferation. Thus, the E8 media was supplemented with the small-molecule ALK5 inhibitor, SB431542 [53]. Finally, VEGF-A and the innate bFGF, which are potent proangionenic growth factors, promoted endothelial cell specification and proliferation through the MAPK signaling pathway [46, 54–56].

Figures 1(c-h) demonstrates phase contrast images of the hiPSCs during the endothelial cell differentiation protocol. Higher magnification phase contrast images are shown in Figure S1. On day -1 hiPSCs were organized into colonies typical of pluripotent stem cells. At the initiation of differentiation (Fig. 1c), the cells re-organized and continued to proliferate into a confluent monolayer. CD31+ endothelial cells were sorted after the differentiation process was complete (day 5) and the ligand-bound magnetic beads could be seen 24 hours after re-plating (Fig. 1h). The sorted endothelial cells exhibited the same “cobblestone” morphology that is typically seen in cultured primary and immortalized endothelial cell lines. These changes in cell morphology and organization throughout the differentiation process demonstrated a distinct transition from pluripotency to the endothelial lineage.

3.2 Characterization of the hiPSCs demonstrates endothelial cell-specific gene expression, phenotype, and stable network formation

The hiPSCs were temporally analyzed for gene expression from the pluripotency stage to the final differentiation stage. Figure 2(a) shows gene expression of pluripotency (*OCT4* and *NANOG*) along with mesoderm (*T*) and endothelial cell lineage markers (*CD34*, *PECAM1*,

CDH5, *KDR*, *FLT1*, and *ENG*). These results demonstrate expression of pluripotency markers *OCT4* and *NANOG* at day -1 and no expression by day 5. Accordingly, the upregulation of early mesoderm marker *T* (Brachyury) was observed 24 hours after differentiation was initiated and little expression was detected by day 5. Increased gene expression for endothelial cell lineage markers *CD34*, *PECAM1* (CD31), *ENG* (CD105), *KDR* (VEGFR2), *FLT1* (VEGFR1), and *CDH5* (VE-CAD) was observed by day 5. The hiPSC's phenotype was characterized with flow cytometry. Figure S2 shows representative histograms for pluripotency markers and endothelial cell lineage markers CD31, VEGFR2 (KDR), and VE-CAD on day -1. Flow cytometry analysis demonstrated the population at the end of differentiation on day 5 was 33% CD31+, 58% VEGFR2 (KDR)+, and 68% VE-CAD+ (Fig. 2(b)). The overall differentiation efficiency for CD31 expression with this method was determined to be 27.8% ± 4.6% with flow cytometry analysis of four different differentiations on separate occasions (Fig. S3). The purified population after two passages was 92% CD31+, 78% VEGFR2 (KDR)+, and 99% VE-Cadherin+ (Fig. 2(b)). Figure 2(c-f) shows the cells stained positive for the endothelial markers CD31, eNOS, VE-CAD, and vWF. Additionally, the purified endothelial cells seven days after magnetic sorting readily took up Ac-LDL within 4 hours of treatment (Fig. 2(g)). Finally, the cells spontaneously formed cord-like networks in a 2D Matrigel angiogenesis assay within 24 hours and, unlike HUVECs used in a the same assay, were stable up to 48 hours in culture (Fig 2(h)). To confirm applicability of the differentiation process across different pluripotent cells, the H9 human embryonic stem cell line was differentiated and the unpurified population was analyzed with flow cytometry and fluorescence microscopy on day 5 (Fig. S4). Similar results were seen with the H9 hESC, with approximately 31% of the unpurified population expressing CD31.

3.3 hiPSC-ECs form capillary-like networks that are responsive to biochemical stimuli within the HyA hydrogel

To validate the ability of the **hiPSC-ECs** encapsulated within the HyA hydrogel to respond to proangiogenic signals, the system was cultured in only EGM2 media (**E**) or in EMG2 with exogenous growth factors VEGF-A (**EV**) or TGF-β1 (**ET**) loaded within the matrix (**HyA-850**). Additionally, to further establish the necessity of biochemical signals for endothelial cell network formation, the system was cultured in RPMI B27 complete medium (**R**), which lacks proangiogenic growth factors. Figure 3 shows confocal images of **hiPSC-EC** networks with the different culture conditions at day 3, 7, and 14 after cell encapsulation. The cells in **HyA-850R** remained rounded and exhibited limited CD31 expression at day 3 and day 7. They appeared to aggregate and slightly elongate by day 14 and recovered some CD31 expression; however, network formation was not observed. The images demonstrate the EC's limited ability to form networks within the matrix in the complete absence of proangiogenic signals. For **HyA-850E**, cell elongation appeared to begin by day 3. Sprouting was observed on day 7, and a stable capillary-like network of vessels was established by day 14. The **HyA-850EV** models exhibited pathological angiogenesis when exogenous VEGF-A was loaded within the hydrogel during cell encapsulation. By day 7 **HyA-850EV** demonstrated a high-density network relative to **HyA-850E**. This capillary-like network was unstable and deteriorated by day 14. The **HyA-850ET** demonstrated cell elongation and sprouting as early as day 3. The hiPSC-ECs

continued to sprout and form nodes by day 7 and a complex capillary-like network was observed by day 14. The quantitative data for total length of the vessel network are shown in Figure 4(a). The quantitative analysis demonstrates that the **HyA-850ET** had a higher total network length than **HyA-850R** and **HyA-850E** on day 3 that was statistically significant. Further, **HyA-850E**, **HyA-850EV**, and **HyA-850ET** all had significantly higher network length than **HyA-850R** at day 7 and 14. Consistent with the fluorescent microscopy, **HyA-850EV** showed a significantly higher network length compared to **HyA-850E** on day 7, but not day 14, indicative of unstable networks. Finally, as seen in the confocal images, **HyA-850E** and **HyA-850ET** maintained significantly higher total network length and demonstrated the most stable tube formation up to day 14 relative to **HyA-850R**.

3.4 Matrix rigidity affects hiPSC-EC network formation and function

The ability of the system to respond to changes in matrix stiffness was evaluated by comparing hiPSC-EC within **HyA-850E** to a less rigid matrix, **HyA-170E**. Figure 4(a) shows the quantitative analysis of the EC networks for 850Pa and 170Pa hydrogels, where for each day the right column represents the 170 Pa hydrogels. We observed early sprouting and tube formation at day 3 in **HyA-170E**. However, this was significantly reduced by day 7, where only elongated cells were observed and no tube formation was detected. Some elongated cells remained at day 14, but no further tube formation occurred in the softer **HyA-170E** compared to the **HyA-850E,** which had a higher shear modulus and showed stable tube formation along with a statistically significant increase in total network length for only **HyA-850E** and **ET** on day 14. Despite being fed EGM2 media, which contains several proangiogenic factors, **HyA-170E** could not support long-term, stable tube formation.

3.5 hiPSC-ECs produce nitric oxide in response to microenvironmental stimuli

The production of NO by the hiPSC-ECs in the **HyA-850** matrix was similar among the different media conditions on day 3 and 7 (Fig. 4(b)). A statistically significant increase in nitric oxide production was found at day 14 in **HyA-850E** matrix, compared to those loaded with exogenous VEGF-A and TGF-βE This finding corresponds with the stable tube formation found in **HyA-850E** at day 14. Cells in **HyA-850E** also demonstrated an overall increase in nitrite concentration from day 7 to day 14.

3.6 hiPSC-EC sprouting was eliminated by treatment with an angiogenesis inhibitor

A dose response study was performed with **HyA-850E** by treating the culture media with the VEGFR2/FGFR small-molecule inhibitor SU5402 for 7 days. Figure 5(a) shows the untreated samples exhibited normal sprouting behavior by day 7. In contrast, the treated groups demonstrated a pronounced decrease in cell elongation at the lowest dose, while angiogenic sprouting was eliminated and only rounded cells remained in the highest dose of 10 μM. Figure 5(b) shows the dose-response curve with a nonlinear regression analysis based on total network length fitted to all experimental replicates. The IC_{50} value was determined to be 0.017 μM, which is in agreement with previously published data that reports an IC_{50} value of 0.02 μM [57].

3.7 hiPSC-ECs encapsulated within HyA matrix and loaded in a microfluidic device demonstrated perfusion of capillary-like network

The patency of the vessel-like networks was demonstrated by loading **HyA-850E** into a tri-chamber microfluidic device intended to create 3D vascular-like fluid flow (Fig 6(a-1,2)) [25, 26, 45]. The hiPSC-ECs formed interconnected tubes with visibly hollow lumen that remained stable throughout the experiment. Fluorescently conjugated Ac-LDL was added to demonstrate the cells remained functional and viable when loaded into the device (Fig. 6(a-3)). The device was then loaded with 2 μm diameter fluorescent microbeads to demonstrate the presence of a perfusable lumen within the networks. Figure 6(b) shows a time-lapse montage of the beads flowing into an open-ended tube (*see*, Suppl. Movie 1). Figure 6(c) shows a high-magnification confocal z-stack image of fluorescent microbeads flowing through the capillary-like tube within the sample.

4. Discussion

In this study, we demonstrated a novel platform combining hiPSC-ECs, a bioinspired hydrogel, and microfluidic testbed to study angiogenesis *in vitro*. The method for differentiating human induced pluripotent stem cells to endothelial cell lineage was refined by using a defined medium (E8) supplemented with proangiogenic factors to direct Wnt, SMAD, and MEK/MAPK pathways that regulate embryonic vasculogenesis and angiogenesis. The differentiation protocol resulted in the sustained expression of endothelial lineage markers so that the terminally differentiated population could be purified based on CD31+ expression. After a week of expansion, the sorted hiPSC-ECs took up Ac-LDL and formed stable networks in a Matrigel angiogenesis assay for up to three days, unlike HUVECs which typically regress within 12-24 hours [3]. The purified population also maintained CD31 and VEGFR2 expression, and increased VE-CAD expression. The hiPSC-EC's ability to perform lineage-specific functions and maintain endothelial marker expression shortly after sorting demonstrated their suitability for assessing the angiogenic potential of biomaterials.

Next, we verified the endothelial cells derived from this differentiation method could be used in a relevant *in vitro* angiogenesis model. The hiPSC-ECs ability to respond to biochemical and biophysical cues within a bioinspired hyaluronic acid matrix was demonstrated by dynamic changes in network formation and nitric oxide production. First, we confirmed that without proangiogenic signals, the encapsulated hiPSC-ECs neither sprouted nor self-assembled into capillary-like networks (HyA-850R). The hiPSC-EC's ability to form stable networks occurred once the system was cultured in the growth factor-rich endothelial growth medium, EGM2 (HyA-850E), which demonstrated the encapsulated hiPSC-ECs were dependent on proangiogenic signaling. The dependence of network formation on specific growth factors could also be modeled with this system by loading the HyA hydrogel with exogenous VEGF-A and TGF-βE The HyA-850EV demonstrated a specific response to the addition of VEGF-A by the formation of a high-density vasculature that had limited stability and regressed by day 14. This reaction has been observed in several other studies where the highest concentration of VEGFA in their hydrogel system yielded a high density but unstable capillary-like network *in vitro*. [4, 58, 59]. This effect has been

extensively reported in the tumor microenvironment where high concentrations of VEGFA promote formation of high density, tortuous, and unstable capillaries [47, 60, 61]. The HyA-850ET system demonstrated the most stable, long-term capillary-like network formation, which was in agreement with previous studies that demonstrated TGF-β1 loaded in the HyA-850 hydrogel promoted capillary-like network formation of mouse cardiac progenitor cells *in vitro* and robust angiogenesis *in vivo* [38]. Similar results were observed in a study with human cardiac progenitor cells, where TGF-β1 signaling through the CD105 co-receptor was found to be key to the formation of vascular network formation [62]. Next, we demonstrated the encapsulated ECs response to changes in matrix rigidity was in congruence with several published studies where slower, but more stable tube formation has been observed in stiffer matrices (e.g. HyA-850E) compared to the softer matrices (e.g. HyA-170E). [38, 58, 63, 64] The current literature suggests that angiogenic sprouting and branching depends on a myriad of parameters including matrix stiffness, pre-polymer concentration, cross-linking density, crosslinking/gelation rates, growth factor retention, adhesion ligand density, matrix degradation rates, and cell type/concentration. [11, 14, 38, 58, 63, 64] A full-factorial analysis of these parameters was done in previous work [36–38] and was beyond the scope of this study, which aimed to demonstrate the ability of the HyA matrix to support a bio-responsive hiPSC-EC *in vitro* angiogenesis model. Nitric oxide (NO) assays in angiogenesis models can aid in determining cell/tissue health, since a decrease in NO production is associated with dysfunctional endothelial cells [60, 65–68]. The Griess assay further validated our system as an *in vitro* model for angiogenesis, since higher NO production was detected in the HyA-850E compared to the hydrogels loaded with significantly higher concentrations of proangiogenic growth factors (HyA-850EV and HyA-850ET).

The dependence of tube formation on proangiogenic signaling and the potential for our angiogenesis model to be used in preclinical toxicology and drug testing was further demonstrated by treating the HyA-850E system with a small-molecule inhibitor of VEGFR2/FGFR (SU5402). Endothelial tube formation was responsive to inhibitor dosage and provided an IC_{50} value that was in agreement with previous reports [57]. Finally, tube patency and perfusion were demonstrated by loading the hiPSC-ECs and HyA-850E hydrogel into a microfluidic device. A vascular network developed that allowed fluid flow within the lumens of the individual vessels, consistent with recent reports using hiPSC-ECs and fibrin as the matrix [32].

5. Conclusions

We demonstrated a novel platform to study angiogenesis *in vitro* by combining hiPSC-ECs with a bioinspired hydrogel and microfluidic testbed. First, we presented a refined method for differentiating hiPSCs into a CD31+ endothelial cell population (hiPSC-ECs), using a single basal medium from the pluripotency stage to the final stage of differentiation. The ability of the hiPSC-ECs obtained from the refined differentiation method to maintain lineage-specific marker expression and function demonstrated their suitability for assessing the angiogenic potential of biomaterials. Subsequently, we showed that a bioinspired HyA hydrogel presented a stable 3D microenvironment for the hiPSC-ECs to respond to biochemical and biophysical cues, which captured, dynamic changes in network formation

and nitric oxide production. The system's sensitivity to microenvironmental changes and 3D capillary-like structure makes the combined platform (i.e., hiPSC derived endothelial cells, HyA matrix, and media) a relevant *in vitro* angiogenesis model for biomaterials development and pre-clinical screening of anti-angiogenic or cardiovascular drugs.

Supplementary Material

Refer to Web version on PubMed Central for supplementary material.

Acknowledgements

This research was supported by NIH grants UH2TR000487 (K. E. H.), UH2TR000487-02S1 (K. E. H.), and UH3TR000487 (K. E. H.). Additionally, this material is based upon work supported by the National Science Foundation Graduate Research Fellowship under Grant No. DGE 1106400. Any opinion, findings, and conclusions or recommendations expressed in this material are those of the authors and do not necessarily reflect the views of the National Science Foundation. S. L.N.-D. was also supported by doctoral fellowships from NIH T32 GM 098218 and the Siebel Scholars Foundation. We acknowledge and thank the U.C. Berkeley Stem Cell Center, Flow Cytometry Core Facilities at U.C. Berkeley, Mary West, Hector Nolla, and Brian Siemens for their assistance with this work.

9. References

[1]. Lalit PA, Hei DJ, Raval AN, and Kamp TJ (2014). Induced pluripotent stem cells for post-myocardial infarction repair: remarkable opportunities and challenges. Circ Res 114, 1328–1345. [PubMed: 24723658]

[2]. Mak IW, Evaniew N, and Ghert M (2014). Lost in translation: animal models and clinical trials in cancer treatment. Am J Transl Res 6, 114–118. [PubMed: 24489990]

[3]. Sanz-Nogues C and O'Brien T (2016). In vitro models for assessing therapeutic angiogenesis. Drug Discov Today 21, 1495–1503. [PubMed: 27262402]

[4]. Chwalek K, Tsurkan MV, Freudenberg U, and Werner C (2014). Glycosaminoglycan-based hydrogels to modulate heterocellular communication in in vitro angiogenesis models. Sci Rep 4, 4414. [PubMed: 24643064]

[5]. Prestwich GD (2011). Hyaluronic acid-based clinical biomaterials derived for cell and molecule delivery in regenerative medicine. J Control Release 155, 193–199. [PubMed: 21513749]

[6]. Prestwich GD, Marecak DM, Marecek JF, Vercruysse KP, and Ziebell MR (1998). Controlled chemical modification of hyaluronic acid: synthesis, applications, and biodegradation of hydrazide derivatives. J Control Release 53, 93–103. [PubMed: 9741917]

[7]. Lorentz KM, Kontos S, Frey P, and Hubbell JA (2011). Engineered aprotinin for improved stability of fibrin biomaterials. Biomaterials 32, 430–438. [PubMed: 20864171]

[8]. Rice JJ, Martino MM, De Laporte L, Tortelli F, Briquez PS, and Hubbell JA (2013). Engineering the regenerative microenvironment with biomaterials. Adv Healthc Mater 2, 57–71. [PubMed: 23184739]

[9]. Anderson SM, Siegman SN, and Segura T (2011). The effect of vascular endothelial growth factor (VEGF) presentation within fibrin matrices on endothelial cell branching. Biomaterials 32, 7432–7443. [PubMed: 21783250]

[10]. Zhu X, Gojgini S, Chen TH, Fei P, Dong S, Ho CM, and Segura T (2017). Directing three-dimensional multicellular morphogenesis by self-organization of vascular mesenchymal cells in hyaluronic acid hydrogels. J Biol Eng 11, 12. [PubMed: 28392831]

[11]. Ronaldson-Bouchard K and Vunjak-Novakovic G (2018). Organs-on-a-Chip: A Fast Track for Engineered Human Tissues in Drug Development. Cell Stem Cell 22, 310–324. [PubMed: 29499151]

[12]. Morin KT and Tranquillo RT (2013). In vitro models of angiogenesis and vasculogenesis in fibrin gel. Exp Cell Res 319, 2409–2417. [PubMed: 23800466]

[13]. Nsair A and MacLellan WR (2011). Induced pluripotent stem cells for regenerative cardiovascular therapies and biomedical discovery. Adv Drug Deliv Rev 63, 324–330. [PubMed: 21371511]

[14]. Briquez P, Clegg Lindsay, Hubbell Jeffrey (2016). Design principles for therapeutic angiogenic materials review. Nature Reviews 1, 1–15.

[15]. Prestwich GD and Healy KE (2015). Why regenerative medicine needs an extracellular matrix. Expert Opin Biol Ther 15, 3–7. [PubMed: 25482878]

[16]. Morgan JP, Delnero PF, Zheng Y, Verbridge SS, Chen J, Craven M, Choi NW, Diaz-Santana A, Kermani P, Hempstead Bv et al. (2013). Formation of microvascular networks in vitro. Nat Protoc 8, 1820–1836. [PubMed: 23989676]

[17]. Nikkhah M, Eshak N, Zorlutuna P, Annabi N, Castello M, Kim K, Dolatshahi-Pirouz A, Edalat F, Bae H, Yang Y, et al. (2012). Directed endothelial cell morphogenesis in micropatterned gelatin methacrylate hydrogels. Biomaterials 33, 9009–9018. [PubMed: 23018132]

[18]. Prakash Parthiban S, Rana D, Jabbari E, Benkirane-Jessel N, and Ramalingam M (2017). Covalently immobilized VEGF-mimicking peptide with gelatin methacrylate enhances microvascularization of endothelial cells. Acta Biomater 51, 330–340. [PubMed: 28110074]

[19]. Zheng Y, Chen J, Craven M, Choi NW, Totorica S, Diaz-Santana A, Kermani P, Hempstead B, Fischbach-Teschl C, Lopez JA, et al. (2012). In vitro microvessels for the study of angiogenesis and thrombosis. Proc Natl Acad Sci U S A 109, 9342–9347. [PubMed: 22645376]

[20]. Badylak SF, Freytes DO, and Gilbert TW (2009). Extracellular matrix as a biological scaffold material: Structure and function. Acta Biomater 5, 1–13. [PubMed: 18938117]

[21]. Saldin LT, Cramer MC, Velankar SS, White LJ, and Badylak SF (2017). Extracellular matrix hydrogels from decellularized tissues: Structure and function. Acta Biomater 49, 1–15. [PubMed: 27915024]

[22]. Burdick JA and Prestwich GD (2011). Hyaluronic acid hydrogels for biomedical applications. Adv Mater 23, H41–56. [PubMed: 21394792]

[23]. Highley CB, Prestwich GD, and Burdick JA (2016). Recent advances in hyaluronic acid hydrogels for biomedical applications. Curr Opin Biotechnol 40, 35–40. [PubMed: 26930175]

[24]. Nih LR, Gojgini S, Carmichael ST, and Segura T (2018). Dual-function injectable angiogenic biomaterial for the repair of brain tissue following stroke. Nat Mater

[25]. Moya ML, Hsu YH, Lee AP, Hughes CC, and George SC (2013). In vitro perfused human capillary networks. Tissue Eng Part C Methods 19, 730–737. [PubMed: 23320912]

[26]. Sobrino A, Phan DT, Datta R, Wang X, Hachey SJ, Romero-Lopez M, Gratton E, Lee AP, George SC, and Hughes CC (2016). 3D microtumors in vitro supported by perfused vascular networks. Sci Rep 6, 31589. [PubMed: 27549930]

[27]. Prokoph S, Chavakis E, Levental KR, Zieris A, Freudenberg U, Dimmeler S, and Werner C (2012). Sustained delivery of SDF-1alpha from heparin-based hydrogels to attract circulating pro-angiogenic cells. Biomaterials 33, 4792–4800. [PubMed: 22483246]

[28]. Bouis D, Hospers GA, Meijer C, Molema G, and Mulder NH (2001). Endothelium in vitro: a review of human vascular endothelial cell lines for blood vessel-related research. Angiogenesis 4, 91–102. [PubMed: 11806248]

[29]. Bray LJ, Binner M, Holzheu A, Friedrichs J, Freudenberg U, Hutmacher DW, and Werner C (2015). Multi-parametric hydrogels support 3D in vitro bioengineered microenvironment models of tumour angiogenesis. Biomaterials 53, 609–620. [PubMed: 25890757]

[30]. Shi Y, Inoue H, Wu JC, and Yamanaka S (2017). Induced pluripotent stem cell technology: a decade of progress. Nat Rev Drug Discov 16, 115–130. [PubMed: 27980341]

[31]. Belair DG, Whisler JA, Valdez J, Velazquez J, Molenda JA, Vickerman V, Lewis R, Daigh C, Hansen TD, Mann DA, et al. (2015). Human vascular tissue models formed from human induced pluripotent stem cell derived endothelial cells. Stem Cell Rev 11, 511–525. [PubMed: 25190668]

[32]. Kurokawa YK, Yin RT, Shang MR, Shirure VS, Moya ML, and George SC (2017). Human Induced Pluripotent Stem Cell-Derived Endothelial Cells for Three-Dimensional Microphysiological Systems. Tissue Eng Part C Methods 23, 474–484. [PubMed: 28622076]

[33]. Manikowski D, Andree B, Samper E, Saint-Marc C, Olmer R, Vogt P, Strauss S, Haverich A, and Hilfiker A (2018). Human adipose tissue-derived stromal cells in combination with exogenous

stimuli facilitate three-dimensional network formation of human endothelial cells derived from various sources. Vascul Pharmacol

[34]. Lian X, Bao X, Al-Ahmad A, Liu J, Wu Y, Dong W, Dunn KK, Shusta EV, and Palecek SP (2014). Efficient differentiation of human pluripotent stem cells to endothelial progenitors via small-molecule activation of WNT signaling. Stem Cell Reports 3, 804–816. [PubMed: 25418725]

[35]. Wilson HK, Canfield SG, Shusta EV, and Palecek SP (2014). Concise review: tissue-specific microvascular endothelial cells derived from human pluripotent stem cells. Stem Cells 32, 3037–3045. [PubMed: 25070152]

[36]. Jha AK, Mathur A, Svedlund FL, Ye J, Yeghiazarians Y, and Healy KE (2015). Molecular weight and concentration of heparin in hyaluronic acid-based matrices modulates growth factor retention kinetics and stem cell fate. J Control Release 209, 308–316. [PubMed: 25931306]

[37]. Jha AK, Tharp KM, Browne S, Ye J, Stahl A, Yeghiazarians Y, and Healy KE (2016). Matrix metalloproteinase-13 mediated degradation of hyaluronic acid-based matrices orchestrates stem cell engraftment through vascular integration. Biomaterials 89, 136–147. [PubMed: 26967648]

[38]. Jha AK, Tharp KM, Ye J, Santiago-Ortiz JL, Jackson WM, Stahl A, Schaffer DV, Yeghiazarians Y, and Healy KE (2015). Enhanced survival and engraftment of transplanted stem cells using growth factor sequestering hydrogels. Biomaterials 47, 1–12. [PubMed: 25682155]

[39]. Rezania A and Healy KE (1999). Integrin subunits responsible for adhesion of human osteoblast-like cells to biomimetic peptide surfaces. J Orthop Res 17, 615–623. [PubMed: 10459771]

[40]. Collins MN and Birkinshaw C (2013). Hyaluronic acid based scaffolds for tissue engineering--a review. Carbohydr Polym 92, 1262–1279. [PubMed: 23399155]

[41]. Xu X, Jha AK, Harrington DA, Farach-Carson MC, and Jia X (2012). Hyaluronic Acid-Based Hydrogels: from a Natural Polysaccharide to Complex Networks. Soft Matter 8, 3280–3294. [PubMed: 22419946]

[42]. Orlova VV, van den Hil FE, Petrus-Reurer S, Drabsch Y, Ten Dijke P, and Mummery CL (2014). Generation, expansion and functional analysis of endothelial cells and pericytes derived from human pluripotent stem cells. Nat Protoc 9, 1514–1531. [PubMed: 24874816]

[43]. Harbers GM and Healy KE (2005). The effect of ligand type and density on osteoblast adhesion, proliferation, and matrix mineralization. J Biomed Mater Res A 75, 855–869. [PubMed: 16121356]

[44]. Chevalier F, Lavergne M, Negroni E, Ferratge S, Carpentier G, Gilbert-Sirieix M, Sineriz F, Uzan G, and Albanese P (2014). Glycosaminoglycan mimetic improves enrichment and cell functions of human endothelial progenitor cell colonies. Stem Cell Res 12, 703–715. [PubMed: 24681520]

[45]. Hsu YHM, M L; Hughes CC; George SC; Lee AP (2013). A microfluidic platform for generating large-scale nearly identical human microphysiological vascularized tissue arrays. Lab Chip 13, 2990–2998. [PubMed: 23723013]

[46]. Chung AS and Ferrara N (2011). Developmental and pathological angiogenesis. Annu Rev Cell Dev Biol 27, 563–584. [PubMed: 21756109]

[47]. Herbert SP and Stainier DY (2011). Molecular control of endothelial cell behaviour during blood vessel morphogenesis. Nat Rev Mol Cell Biol 12, 551–564. [PubMed: 21860391]

[48]. Patel-Hett S and D'Amore PA (2011). Signal transduction in vasculogenesis and developmental angiogenesis. Int J Dev Biol 55, 353–363. [PubMed: 21732275]

[49]. Lian X, Hsiao C, Wilson G, Zhu K, Hazeltine LB, Azarin SM, Raval KK, Zhang J, Kamp TJ, and Palecek SP (2012). Robust cardiomyocyte differentiation from human pluripotent stem cells via temporal modulation of canonical Wnt signaling. Proc Natl Acad Sci U S A 109, E1848–1857. [PubMed: 22645348]

[50]. Shi Y and Massague J (2003). Mechanisms of TGF-beta signaling from cell membrane to the nucleus. Cell 113, 685–700. [PubMed: 12809600]

[51]. Bertolino P, Deckers M, Lebrin F, and ten Dijke P (2005). Transforming growth factor-beta signal transduction in angiogenesis and vascular disorders. Chest 128, 585S–590S. [PubMed: 16373850]

[52]. Lebrin F, Deckers M, Bertolino P, and Ten Dijke P (2005). TGF-beta receptor function in the endothelium. Cardiovasc Res 65, 599–608. [PubMed: 15664386]

[53]. Inman GJ, Nicolas FJ, Callahan JF, Harling JD, Gaster LM, Reith AD, Laping NJ, and Hill CS (2002). SB-431542 is a potent and specific inhibitor of transforming growth factor-beta superfamily type I activin receptor-like kinase (ALK) receptors ALK4, ALK5, and ALK7. Mol Pharmacol 62, 65–74. [PubMed: 12065756]

[54]. Ferrara N, Gerber HP, and LeCouter J (2003). The biology of VEGF and its receptors. Nat Med 9, 669–676. [PubMed: 12778165]

[55]. Marcelo KL, Goldie LC, and Hirschi KK (2013). Regulation of endothelial cell differentiation and specification. Circ Res 112, 1272–1287. [PubMed: 23620236]

[56]. Farnsworth RH, Lackmann M, Achen MG, and Stacker SA (2014). Vascular remodeling in cancer. Oncogene 33, 3496–3505. [PubMed: 23912450]

[57]. Sun L, Tran N, Liang C, Tang F, Rice A, Schreck R, Waltz K, Shawver LK, McMahon G, and Tang C (1999). Design, synthesis, and evaluations of substituted 3-[(3- or 4-carboxyethylpyrrol-2-yl)methylidenyl]indolin-2-ones as inhibitors of VEGF, FGF, and PDGF receptor tyrosine kinases. J Med Chem 42, 5120–5130. [PubMed: 10602697]

[58]. Zanotelli MR, Ardalani H, Zhang J, Hou Z, Nguyen EH, Swanson S, Nguyen BK, Bolin J, Elwell A, Bischel LL, et al. (2016). Stable engineered vascular networks from human induced pluripotent stem cell-derived endothelial cells cultured in synthetic hydrogels. Acta Biomater 35, 32–41. [PubMed: 26945632]

[59]. Ozawa CR, Banfi A, Glazer NL, Thurston G, Springer ML, Kraft PE, McDonald DM, and Blau HM (2004). Microenvironmental VEGF concentration, not total dose, determines a threshold between normal and aberrant angiogenesis. J Clin Invest 113, 516–527. [PubMed: 14966561]

[60]. Carmeliet P and Jain RK (2011). Principles and mechanisms of vessel normalization for cancer and other angiogenic diseases. Nat Rev Drug Discov 10, 417–427. [PubMed: 21629292]

[61]. Hanahan D and Weinberg RA (2011). Hallmarks of cancer: the next generation. Cell 144, 646–674. [PubMed: 21376230]

[62]. Browne S, Jha AK, Ameri K, Marcus SG, Yeghiazarians Y, and Healy KE (2018). TGF-beta1/CD105 signaling controls vascular network formation within growth factor sequestering hyaluronic acid hydrogels. PLoS One 13, e0194679. [PubMed: 29566045]

[63]. Bordeleau F, Mason BN, Lollis EM, Mazzola M, Zanotelli MR, Somasegar S, Califano JP, Montague C, LaValley DJ, Huynh J, et al. (2017). Matrix stiffening promotes a tumor vasculature phenotype. Proc Natl Acad Sci U S A 114, 492–497. [PubMed: 28034921]

[64]. LaValley D and Reinhart-King C (2014). Matrix stiffening in the formation of blood vessels. Advances in Regenerative Biology 1, 1–4.

[65]. Fukumura D, Kashiwagi S, and Jain RK (2006). The role of nitric oxide in tumour progression. Nat Rev Cancer 6, 521–534. [PubMed: 16794635]

[66]. Gimbrone MA Jr. and Garcia-Cardena G (2016). Endothelial Cell Dysfunction and the Pathobiology of Atherosclerosis. Circ Res 118, 620–636. [PubMed: 26892962]

[67]. Kelm M (1999). Nitric oxide metabolism and breakdown. Biochim Biophys Acta 1411, 273–289. [PubMed: 10320663]

[68]. Tousoulis D, Kampoli AM, Tentolouris C, Papageorgiou N, and Stefanadis C (2012). The role of nitric oxide on endothelial function. Curr Vasc Pharmacol 10, 4–18. [PubMed: 22112350]

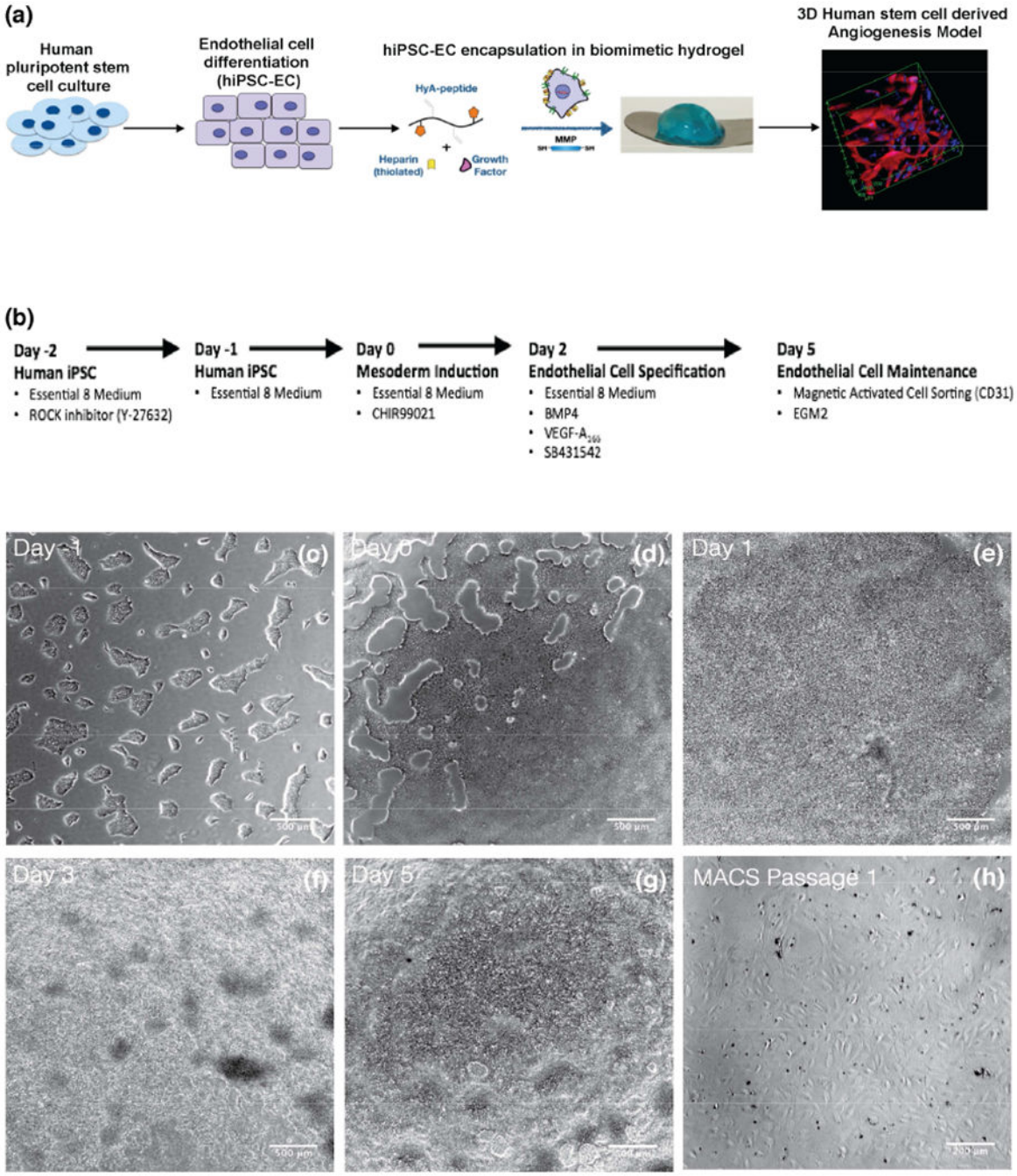

Figure 1.

Endothelial Cell (EC) Differentiation and hydrogel encapsulation. (a) Schematic for the development of the 3D Angiogenesis model starting from the differentiation of hiPSC to ECs and encapsulation within the biomimetic acrylated hyaluronic acid hydrogel (HyA). (b) Endothelial cell differentiation protocol. (c) Phase contrast images demonstrated temporal changes in organization and morphology of the hiPSCs undergoing endothelial cell differentiation.

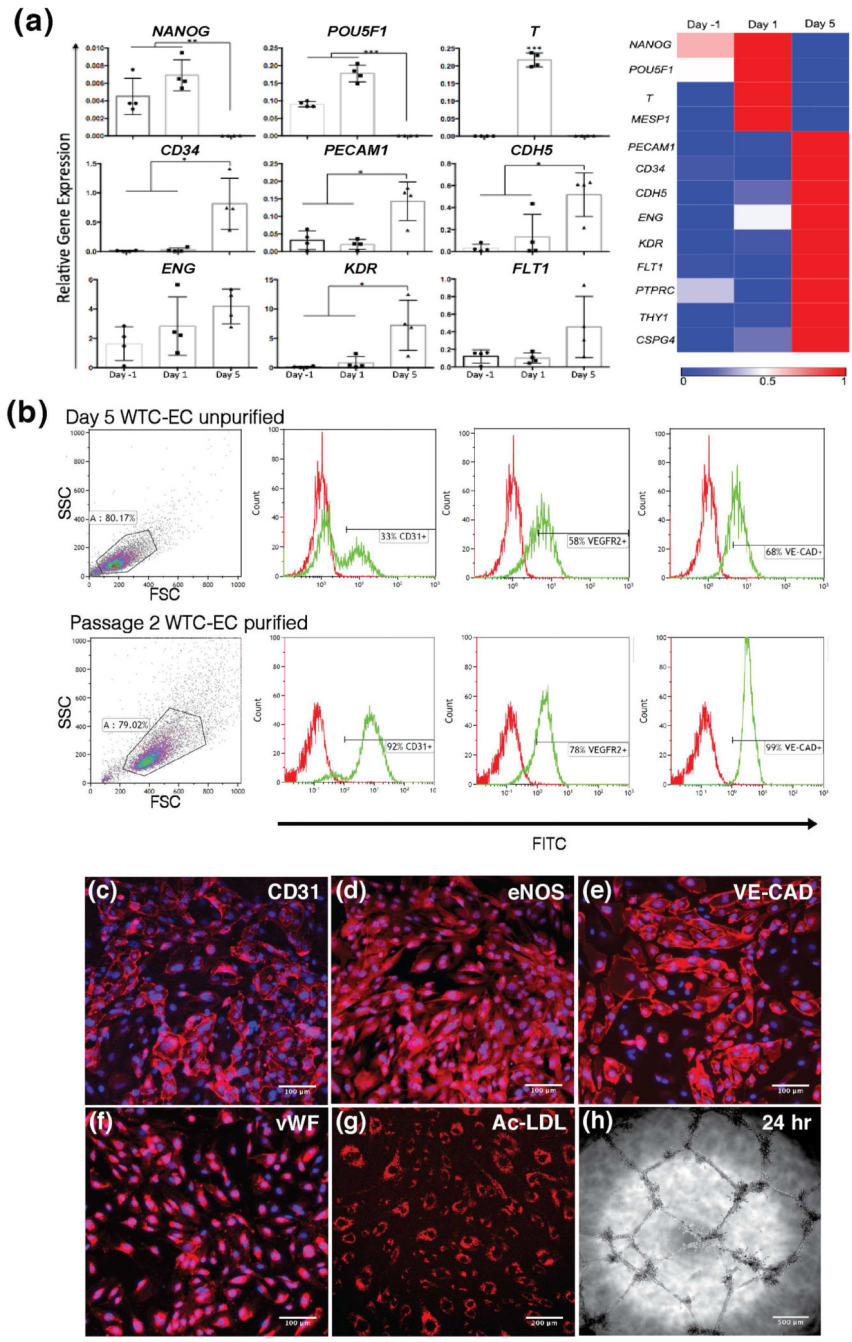

Figure 2.

Characterization of Endothelial Cell population after differentiation and MACS purification. (a) Reverse Transcription quantitative PCR (RT-qPCR) analysis of hiPSCs during endothelial cell differentiation. * $p<0.05$, ** $p<0.01$, *** $p<0.001$ (b) Representative flow cytometry histograms of CD31, VEGFR2, and VE-CAD expression at day 5 and after purification. (c-g) Immunofluorescence staining of CD31+ MACS purified endothelial cells revealed cobblestone morphology, expression of EC-specific markers, and Ac-LDL uptake. (f) Matrigel angiogenesis assay demonstrated stable network formation.

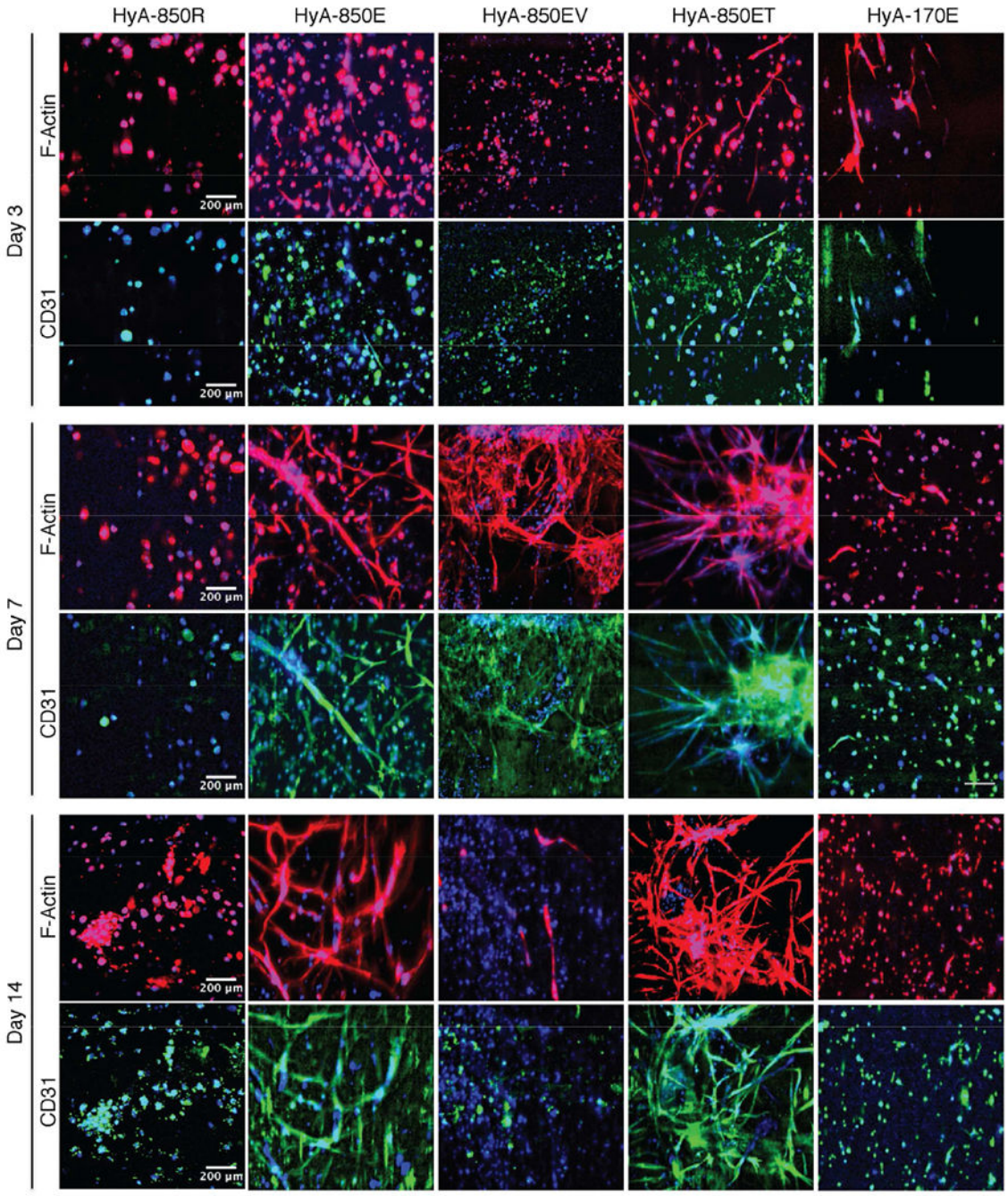

Figure 3.

Analysis of *in vitro* 3D Angiogenesis model with confocal microscopy. Representative confocal z-stack images of hiPSC-ECs encapsulated in acrylated HyA hydrogel stained for F-actin and CD31 at day 3, 7, 14 demonstrated capillary-like network formation and stability dependent on biochemical signals and matrix rigidity.

HyA-850R = 3wt% HyA +WTC hiPSC-EC+RPMI B27 complete media

HyA-850E = 3wt% HyA +WTC hiPSC-EC+EGM2 media

HyA-850ET = 3wt% HyA +WTC hiPSC-EC+EGM2 media + TGFβ1 (gel)

HyA-850EV= 3wt% AcHyA +WTC hiPSC-EC+EGM2 media + VEGF-A (gel)
HyA-170E = 2wt% AcHyA +WTC hiPSC-EC+EGM2 media

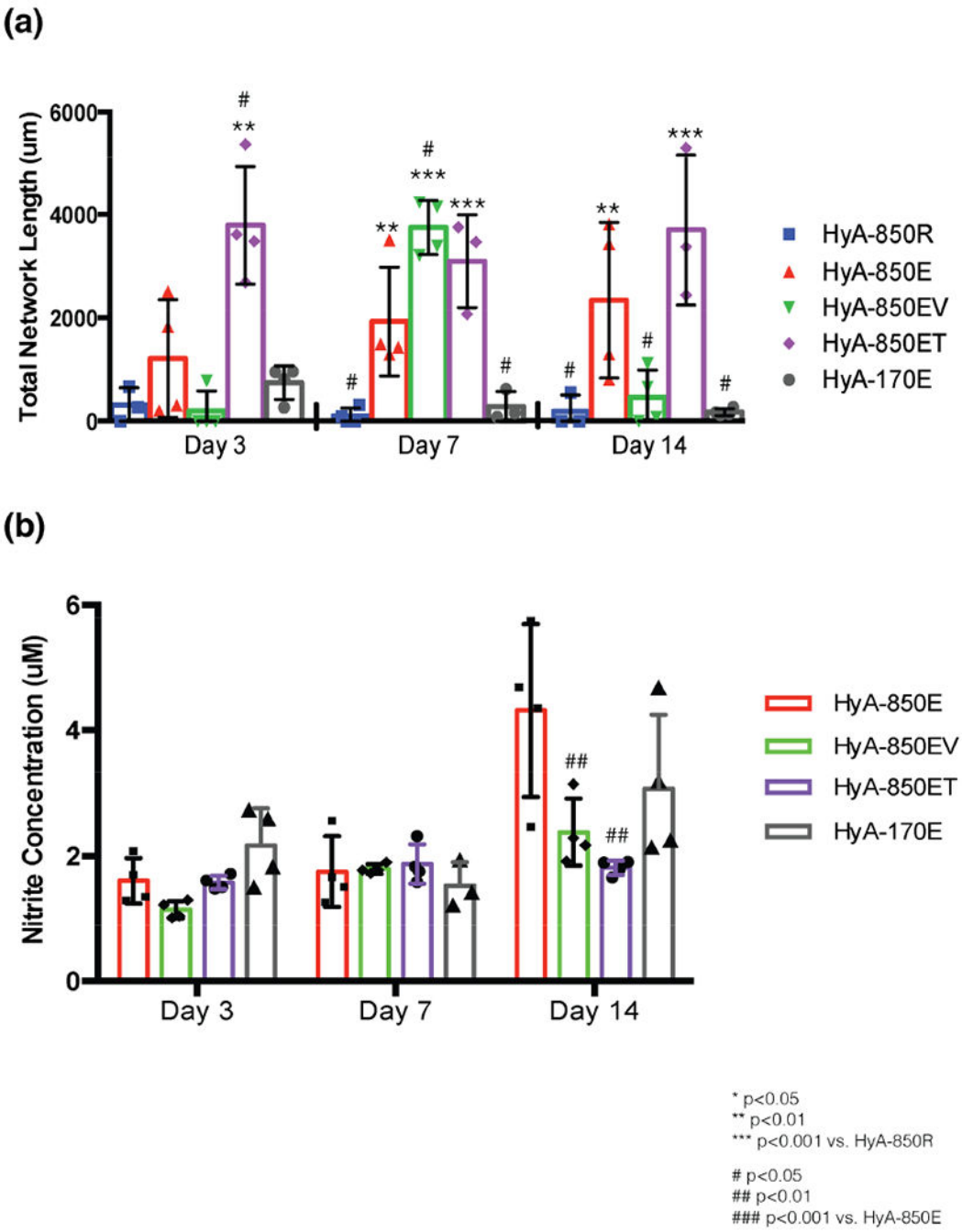

Figure 4.

Quantification of *in vitro* 3D Angiogenesis model network formation and nitric oxide production (a) Analysis of total network length in confocal images demonstrated proangiogenic signals are required for tube formation and stability; analysis of total network length relative to matrix stiffness demonstrated matrix with higher shear modulus formed significantly more tubes that are stable at 2 weeks compared to the softer matrix. (b) Highest nitric oxide production, an indicator of endothelial cell function, corresponded with

HyA-850E which demonstrated greatest tube formation with long-term stability. * $p<0.05$, ** $p<0.01$, *** $p<0.001$ vs. HyA-850R; # $p<0.05$, ## $p<0.01$, ### $p<0.001$ vs. HyA-850E

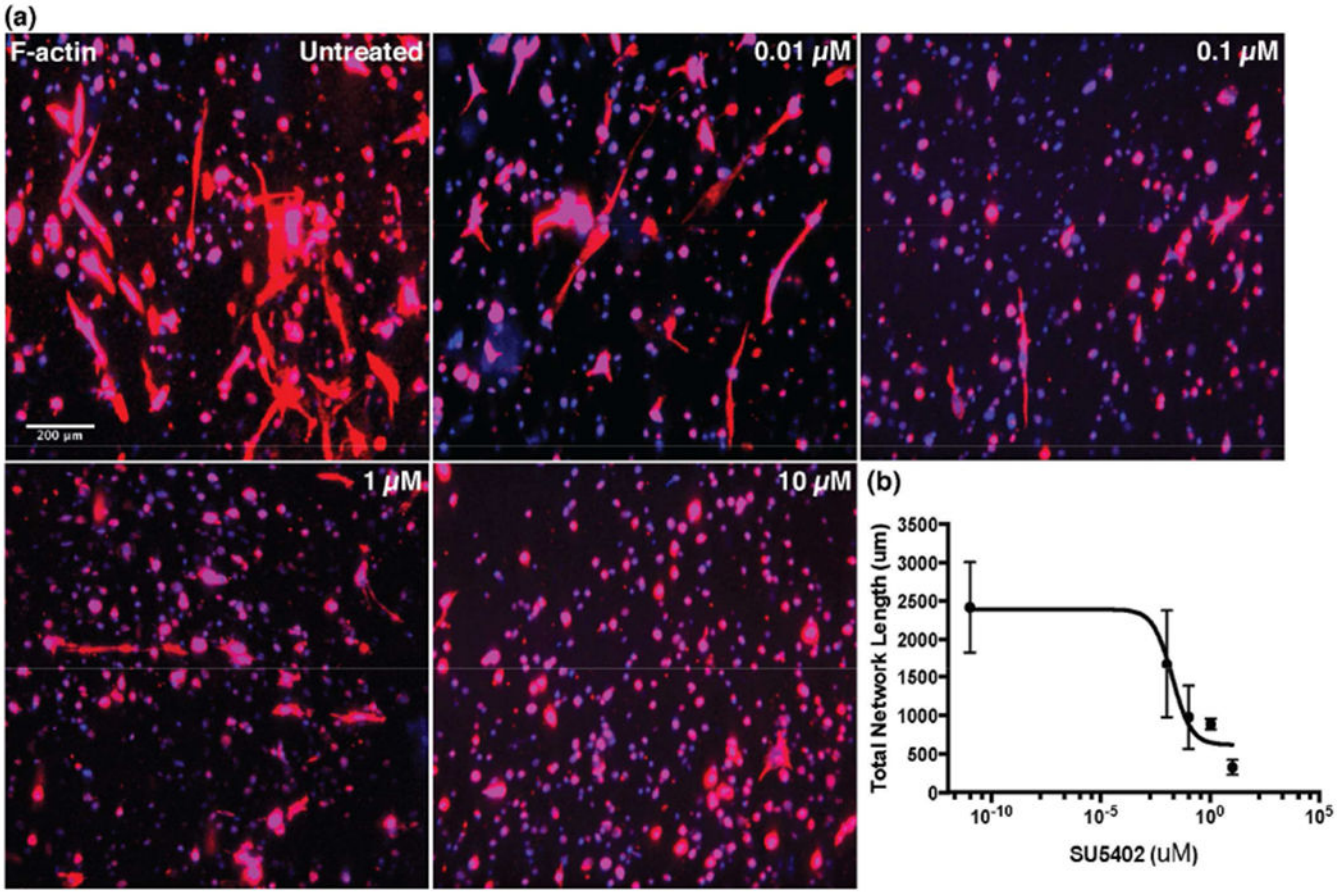

Figure 5.

hiPSC-EC sprouting was eliminated by treatment with small-molecule angiogenesis inhibitor for 7 days after hydrogel encapsulation. (a) Confocal images, (b) IC_{50} value determined from dose-response curve was in agreement with previously published data.

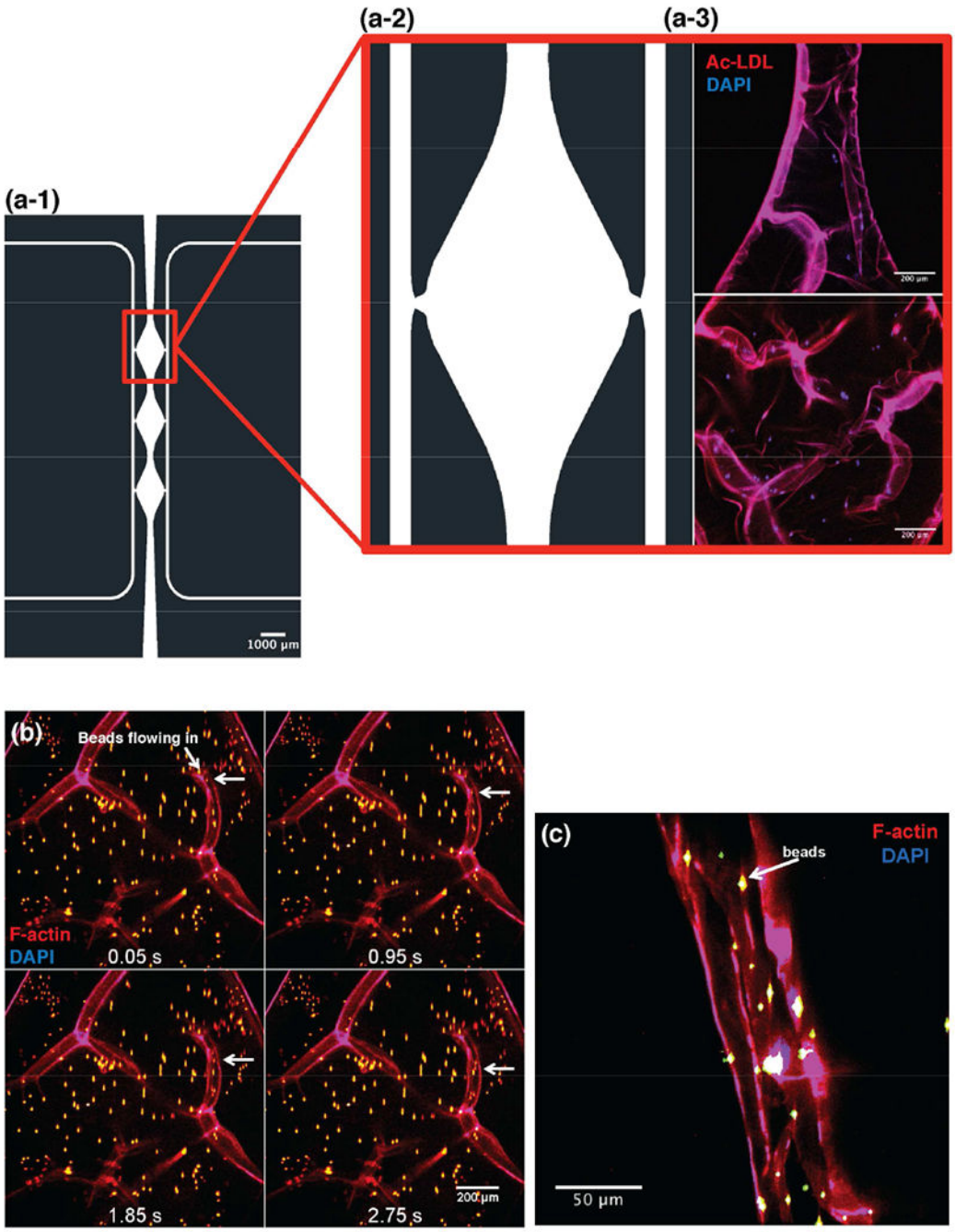

Figure 6.

Cultured HyA-850E in tri-chamber microfluidic device. (a-1) Schematic of device design. (a-2) Magnified image of diamond-shaped sample chamber with flanking media channels, and (a-3) confocal image of fixed HyA-850E loaded into device demonstrated functional capillary-like networks. (b) Time-lapse montage of 2 μm diameter fluorescent microbeads flowing into fixed sample stained for F-actin demonstrated networks are hollow and perfusable (images derived from Supplementary Movie 1). (c) high-magnification confocal

z-stack image of fluorescent microbeads flowing through capillary-like tube within HyA-850E.